Using the shortwave infrared to image middle ear pathologies

Jessica A. Carr[a], Tulio A. Valdez[b,c,1], Oliver T. Bruns[a], and Moungi G. Bawendi[a,1]

[a]Department of Chemistry, Massachusetts Institute of Technology, Cambridge, MA 02139; [b]Otolaryngology–Head and Neck Surgery, University of Connecticut Health Center, Farmington, CT 06269; and [c]Otolaryngology–Head and Neck Surgery, Connecticut Children's Medical Center, Hartford, CT 06106

Contributed by Moungi G. Bawendi, July 1, 2016 (sent for review February 11, 2016; reviewed by Aristides Arrenberg and Aino Ruohola)

Visualizing structures deep inside opaque biological tissues is one of the central challenges in biomedical imaging. Optical imaging with visible light provides high resolution and sensitivity; however, scattering and absorption of light by tissue limits the imaging depth to superficial features. Imaging with shortwave infrared light (SWIR, 1–2 μm) shares many advantages of visible imaging, but light scattering in tissue is reduced, providing sufficient optical penetration depth to noninvasively interrogate subsurface tissue features. However, the clinical potential of this approach has been largely unexplored because suitable detectors, until recently, have been either unavailable or cost prohibitive. Here, taking advantage of newly available detector technology, we demonstrate the potential of SWIR light to improve diagnostics through the development of a medical otoscope for determining middle ear pathologies. We show that SWIR otoscopy has the potential to provide valuable diagnostic information complementary to that provided by visible pneumotoscopy. We show that in healthy adult human ears, deeper tissue penetration of SWIR light allows better visualization of middle ear structures through the tympanic membrane, including the ossicular chain, promontory, round window niche, and chorda tympani. In addition, we investigate the potential for detection of middle ear fluid, which has significant implications for diagnosing otitis media, the overdiagnosis of which is a primary factor in increased antibiotic resistance. Middle ear fluid shows strong light absorption between 1,400 and 1,550 nm, enabling straightforward fluid detection in a model using the SWIR otoscope. Moreover, our device is easily translatable to the clinic, as the ergonomics, visual output, and operation are similar to a conventional otoscope.

shortwave infrared | optical imaging | endogenous contrast | otoscopy | otitis media

Optical imaging and spectroscopy are well-established methods of investigating tissues in vivo and have proven valuable for many diagnostic applications (1–3). A biological tissue sample is illuminated with light and the structural composition and function of the sample can be determined from the diffusely reflected or transmitted light. Equipment for optical measurements is often simple and portable, interrogations can be carried out without contacting or perturbing the tissue over a wide field of view, and the resulting data are generally easy to interpret, all of which have made optical imaging a powerful technique in clinical settings (1, 4). Most optical imaging thus far uses visible and/or near infrared (NIR) light between 400 and 1,000 nm, which can be detected with inexpensive silicon-based sensors. In this wavelength region, oxygenated and deoxygenated hemoglobin are the primary physiologically active optical absorbers, and the functional status of tissue can be measured based on their relative concentrations (5–8).

Extending optical measurements into the shortwave infrared (SWIR; 1,000–2,000 nm) offers several advantages over visible and NIR imaging for certain in vivo applications (3, 9–11). The SWIR regime features absorption from tissue constituents such as water (near 1,150, 1,450, and 1,900 nm), lipids (near 1,040, 1,200, 1,400, and 1,700 nm), and collagen (near 1,200 and 1,500 nm) that are more prominent than corresponding features in the visible and NIR regions (12). The enhanced sensitivity to these chromophores enables better characterization of changes in their concentration, with recent spectroscopy-based examples in detecting and monitoring cancerous tissues (13–15), burns (3), and intestinal ischemia (16), distinguishing skin bruises from surrounding tissue (17, 18), and discriminating histologically vulnerable and stable plaques of blood vessels in vivo (19–21). In addition, SWIR light offers greater transmission through biological tissue than visible or NIR light due to decreased scattering of photons (9, 22, 23). SWIR light thus provides sufficient optical penetration depth to noninvasively interrogate changes in subsurface tissue features, whereas most visible and NIR imaging is limited to superficial structures (11, 22).

Despite these advantages, the SWIR regime has thus far been underused in optical imaging, and in particular, medical devices have been mostly limited to exploratory or proof-of-principle in nature. The limited development of SWIR technology is in part due to the cost-prohibitive nature of nonsilicon semiconductor detector arrays and restricted access due to national defense-related policies such as International Traffic in Arms Regulations (ITAR). However, recent technological advances and an increasing supply of SWIR detectors has enabled a price drop of roughly an order of magnitude over the time period from 2010 to 2014 (12). Advances in detector fabrication have also produced high performing sensors with significantly smaller form factors and reduced weight. Based on such a newly available sensor, we

Significance

Imaging with shortwave infrared (SWIR) light has great potential for visualizing biological structures previously undetectable with visible light. To demonstrate the clinical potential of SWIR imaging, we developed a medical otoscope sensitive to SWIR light. We show that the unique transmission of SWIR light through tissue improves resolution of anatomical structures lying behind thin tissue membranes like the ear drum. We therefore significantly improve imaging of underlying middle ear anatomy. SWIR imaging also allows identification of disease characterized by fluid accumulation, as in the diagnosis of otitis media. With successful diagnosis of otitis media estimated at 51% for US pediatricians, objectifying this diagnosis could curb the antibiotic resistance associated with an estimated 2 million overdiagnoses each year.

Author contributions: J.A.C., T.A.V., O.T.B., and M.G.B. designed research; J.A.C. and T.A.V. performed research; J.A.C. and O.T.B. analyzed data; and J.A.C. wrote the paper.

Reviewers: A.A., University of Tubingen, Center for Integrated Neuroscience; and A.R., University of Turku.

Conflict of interest statement: A patent application has been filed that may lead to monetary compensation to the investigators and/or involved institutions at some point in the future.

[1]To whom correspondence may be addressed. Email: tvaldez@connecticutchildrens.org or mgb@mit.edu.

This article contains supporting information online at www.pnas.org/lookup/suppl/doi:10.1073/pnas.1610529113/-/DCSupplemental.

show here an application of SWIR light in a medical otoscope for evaluating transtympanic middle ear pathologies.

Visible light-based pneumotoscopes have been the diagnostic workhorse for external auditory canal and middle ear examination for over a century. Using this tool, physicians assess middle ear pathologies based on the appearance of the tympanic membrane, or ear drum, and its mobility against hand-generated pneumatic pressure. The pneumotoscope serves as an initial means of identifying tympanic membrane perforations, causes of conductive hearing loss, and most commonly, otitis media, which refers to a continuum of inflammatory conditions of the middle ear including acute infection. Otitis media is second in frequency only to acute upper respiratory infection as the most common illness diagnosed in US children; at least 80% of children will have experienced one or more episodes of otitis media by the age of 3 y (24–27).

However, otoscopic examinations are known to have subjective interpretations, especially in the hands of inexperienced practitioners (28, 29). Successful diagnosis of otitis media is estimated at 51% for US pediatricians, with overdiagnosis of acute otitis media (false positives) occurring 26% of the time (30–32). The resulting variation in antibiotic therapy has made otitis media a primary factor in increased antibiotic resistance (33–35). On the other hand, failure to diagnose otitis media can lead to long-term hearing impairment, intracranial complications, a delay in language acquisition, or formation of destructive skin growths, known as cholesteatoma, which can only be treated by surgical excision (36–39). The limitations of pneumotoscopy are related in part to the thickness of the tympanic membrane, which despite being semitranslucent, reflects, absorbs, and scatters incident light at the surface, limiting signal penetration to deeper middle ear structures or fluid. A study by Rosenfeld of 135 acute otitis media cases diagnosed by US primary care practitioners found that 40 were false positive, 35 of which had no middle ear effusion (40).

Here we describe the development of an otoscope sensitive to SWIR light for more objective diagnoses of transtympanic middle ear pathologies. A SWIR otoscope maintains the ergonomics, visual output, and small footprint of a conventional otoscope, making it easily translatable to the clinic. Meanwhile, SWIR endogenous contrast provides a unique image that can be applied to the identification of middle ear abnormalities. Deeper tissue penetration is achievable with SWIR light than with visible light, allowing better visualization of middle ear structures through the tympanic membrane. A clearer view of these structures would aid in identifying causes of conductive hearing loss. In addition, strong SWIR light absorption of water provides more evident contrast between the presence and absence of optically dense middle ear effusions, which could aid in the diagnosis of otitis media. Therefore, a SWIR otoscope could complement conventional pneumotoscopic diagnoses by providing access to the inherent optical properties of the middle ear across an extended wavelength range.

Results

Light Attenuation of Human Tympanic Membrane Tissue. To predict the performance of a SWIR otoscope in vivo, we investigated the optical properties of human tympanic membrane tissue. Spectroscopic characterization verifies decreasing light attenuation with increasing wavelength (Fig. 1*A*), which is consistent with the inverse power law relationship between wavelength and scattering of photons measured previously for skin (22, 23). The enhanced transmission of SWIR light is advantageous for an otoscope, given that light must pass through the tympanic membrane after reflecting off of the middle ear structures, such as the highly reflective ossicles and the promontory, before being detected. Any absorption or scattering of light by the tympanic membrane inevitably decreases the amount of light that can be delivered to the middle ear structures and further decreases the reflected signal intensity as it traverses back to the detector. However, more importantly, scattering decreases image contrast and resolution as

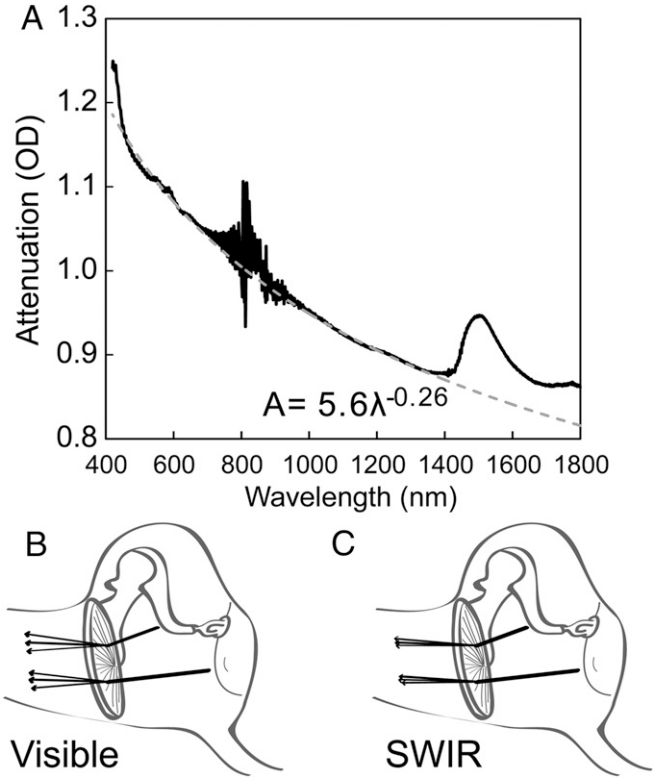

Fig. 1. Attenuation of human tympanic membrane tissue. As wavelength increases, light scattering by the tissue decreases, causing attenuation to decline proportional to the inverse power law $\lambda^{-0.26}$ (*A*, dashed gray line). Absorption by water in the tissue causes attenuation around 1,440 nm and absorption by hemoglobin causes small features at 540 and 575 nm. Noise in the spectrum around 800 nm is due to poor detector sensitivity and grating efficiency in this region under conditions of low light transmission. The spectrum indicates that light reflected by the middle ear ossicles and promontory would scatter less through the tympanic membrane for SWIR light (*C*) compared with visible light (*B*), resulting in greater visibility (Fig. S1).

reflected light travels indirectly through the tympanic membrane to the detector (Fig. 1 *B* and *C*, *SI Results*, and Fig. S1).

Absorption beyond 1,300 nm is also evident in the tympanic membrane attenuation spectrum due to water in the tissue. Although this absorption attenuates overall signal, it does not decrease image contrast and resolution. Even considering the absorption by water, the overall transparency of the tympanic membrane is greater at SWIR wavelengths than in the visible.

Noninvasive SWIR Imaging of Human Middle Ear Anatomy. To take advantage of the decreased light scattering of SWIR light, we designed an SWIR otoscope prototype capable of imaging the middle ear from 900 to 1,700 nm (Fig. 2). Using a 5.0-mm speculum, the device images an ∼10.5-mm-diameter circular field of view with maximum resolution of 45 μm (Fig. S2).

We tested in vivo performance of the SWIR otoscope on ten adults (18 ears) and show that the increased penetration of SWIR light through the tympanic membrane enables the SWIR otoscope to image middle ear anatomy with exceptional detail compared with visible otoscopy (Fig. 3, Figs. S3 and S4, and Table S1 summarize the results). In a typical visible examination, the only clearly identifiable features besides the tympanic membrane are those that are large or superficial, such as the cochlear promontory (15/18 cases), which is formed by the outward projection of the first turn of the cochlea against the posterior wall of the middle ear cavity, and the malleus (18/18 cases), which lies directly under the tympanic membrane. In a few cases, the tympanic membrane is thinner,

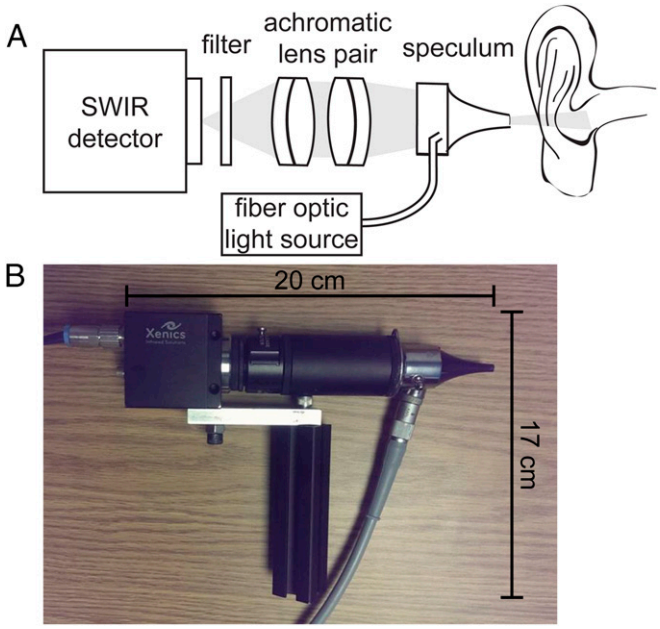

Fig. 2. Schematic and image of the SWIR otoscope. The SWIR otoscope prototype is composed of a compact InGaAs SWIR detector, a filter holder, a pair of achromatic doublet lenses, a fiber-coupled light source, and a disposable medical speculum (*A*). The device is 20 × 17 × 5 cm in size and weighs ~500 g (*B*).

and light reflection off of smaller or deeper anatomy such as the incus (9/18 cases), stapes (2/18 cases), and stapedial tendon (2/18) is identifiable.

The SWIR otoscope, on the other hand, images landmarks of the entire ossicular chain (middle ear bones) (Movie S1), including the incus and stapes (16/18 and 11/18 cases, respectively), in addition to the malleus (18/18 cases). In 12 of 18 cases, it was also possible to image the supporting stapedial tendon. Besides the ossicular chain, the SWIR otoscope can also clearly image the cochlear promontory (18/18 cases), and visualization of the round window niche—one of the two openings from the middle ear to the inner ear—was also achieved (16/18 cases). Furthermore, the SWIR otoscope could identify the chorda tympani (9/18 cases), a branch of the facial nerve that carries taste sensation from the anterior two-thirds of the tongue. The location of the chorda tympani is generally obstructed by a thicker region of the tympanic membrane with visible imaging (visible in 4/18 cases).

Thus, the SWIR otoscope enables visualization of anatomical features that would normally be undetectable due to poor transmission of visible light through the tympanic membrane. For those middle ear structures already detectable by visible examination, the SWIR otoscope further improves the contrast of these features; we show that the contrast of the incus is enhanced by two times on average for the round window and four times on average for the incus (Fig. S5 and *SI Results*).

Light Attenuation of Middle Ear Fluid. As otitis media is the most common pathology observed with an otoscope, we investigated the potential of SWIR light to improve the accuracy of this diagnosis. One of the greatest challenges in the diagnosis of otitis media is the reliable identification of fluid accumulation, or effusion, behind the tympanic membrane in the middle ear. When middle ear effusion is accompanied by rapid onset of one or more signs or symptoms of infection, such as fever, pain and/or irritability, the patient is diagnosed with acute otitis media and treatment with antibiotics is indicated. We acquired several human middle ear fluid samples of a variety of consistencies, ranging from serous to mucoid, to assess their optical characteristics and determine at which wavelength the greatest optical contrast can be achieved.

Spectroscopic characterization confirms strong attenuation of specific spectral bands of SWIR light (Fig. 4). Water in the fluid gives rise to absorption observed in small features around 970 and 1,180 nm and strong features around 1,440 nm and beyond 1,800 nm, corresponding to the vibrational overtone of the O-H bond, and the first overtone of O-H stretching, respectively. Thicker-consistency mucoid middle ear fluid samples contain less water relative to thin samples, but water absorption is still the dominant cause of attenuation (Fig. S6). Two peaks are also distinguishable at 540 and 575 nm from the absorption of oxygenated hemoglobin, but middle ear fluid generally appears translucent by eye due to minimal absorption of chromophores at visible wavelengths (see Fig. S7 for variation in hemoglobin

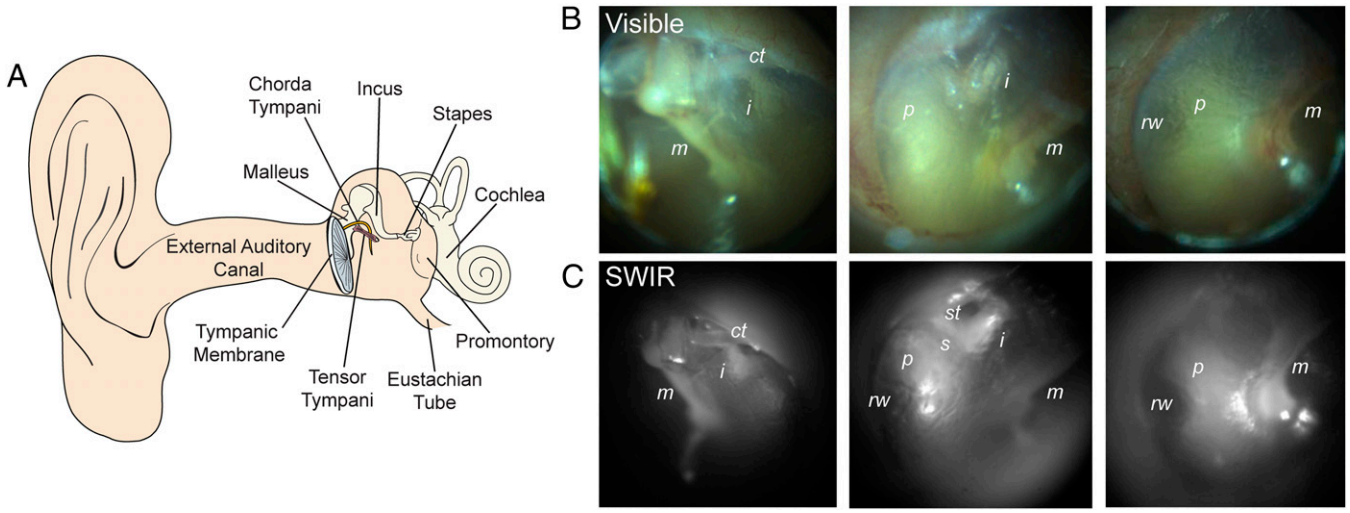

Fig. 3. Schematic of the middle ear and comparison between SWIR and visible examinations in healthy adults. Representative images from examinations of 10 healthy adult humans are shown. Under visible examination, all anatomy besides the malleus is obstructed by the tympanic membrane (*B*). Using the SWIR otoscope, the chorda tympani, malleus, incus, stapes, stapedial tendon, cochlear promontory, and round window niche (indicated by *ct, m, i, s, st, p,* and *rw*, respectively, and shown schematically in *A*) are all clearly identifiable (*C*). See Fig. S3 for outlines of the anatomical features and Fig. S4 for additional SWIR images.

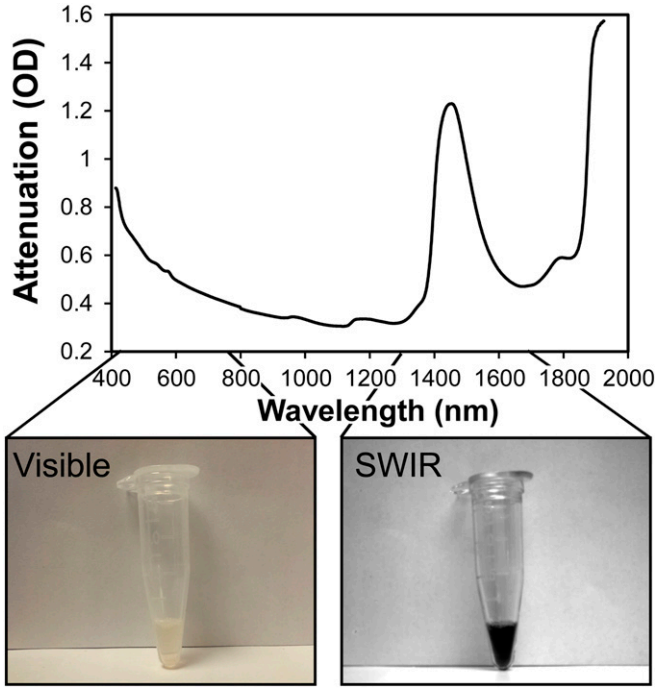

Fig. 4. Optical properties of human middle ear fluid. The attenuation of light through a sample of middle ear fluid shows strong absorption between 1,400 and 1,550 nm due to water content. This absorption of SWIR light causes the fluid to appear black in a SWIR image, whereas it is translucent with visible imaging or by eye.

content). Light scattering processes that occur within the viscous mucous also cause attenuation, particularly at visible wavelengths of light (400–700 nm). The strength of this wavelength dependence is a complicated function of the geometry of the scattering particles, which vary with the composition of individual fluid samples; however, in general, the attenuation steadily rises with decreasing wavelength. In the thickest samples, attenuation is as strong at visible wavelengths due to scattering, as it is in the SWIR due to water absorption.

We therefore expect SWIR wavelengths to provide better optical contrast than visible and NIR imaging in the detection of middle ear fluid, due to the strong absorption endogenous to water in the fluid, regardless of fluid consistency.

Detection of Middle Ear Fluid Phantom in a Middle Ear Model. We evaluated the effectiveness of the SWIR otoscope at detecting fluid by imaging fluid in a 3D-printed middle ear model (Fig. 5). In our model, orange juice was selected as a phantom for middle ear fluid, as it has representative spectroscopic properties, particularly the dominant water absorption features and scattering of visible wavelengths of light (Fig. S8). Using visible otoscopy, slow addition of fluid into the ear model is barely perceptible (Movie S2); reflected light intensity from the middle ear space decreases by less than 30% (Fig. S9*A*). The malleus, which is a superficial anatomical structure, experiences relatively less change in intensity as fluid is added. As a result, the Weber contrast of this feature, defined as the difference between the feature intensity and the background intensity all divided by the background intensity, is doubled from 0.36 to 0.72 when the malleus is surrounded with fluid (Fig. 5*C*).

In contrast, using a 1,300-nm long-pass filter and SWIR detection, the SWIR otoscope can selectively image between 1,300 and 1,700 nm where absorption of middle ear fluid is maximal. Addition of fluid to the model (Movie S3) obstructs any features lying behind the superficial structures at the tympanic membrane and reduces the overall reflected light intensity by nearly 75% (Fig. 5*B* and Fig. S9*B*). This notable intensity reduction causes contrast of the malleus to increase fourfold from 0.30 to 1.2 when surrounded by fluid (Fig. 5*D*)—a significant improvement over the visible case (Fig. 5*E*).

Based on these models and spectroscopic characterization, we therefore expect the imaging contrast of middle ear fluid in vivo to be significantly enhanced with SWIR light compared with what is currently available with visible otoscopy. The relative level of SWIR absorption, which provides a striking contrast, could facilitate a clinician's determination of the absence or presence of fluid in the middle ear.

Discussion

We developed an otoscope sensitive to SWIR light for middle ear disease diagnostics. We show that deeper tissue penetration of SWIR light enhances contrast and enables better visualization of middle ear anatomy through the thin tissue of the tympanic membrane. Although the middle ear anatomy is obfuscated by the tympanic membrane during visible light examinations, SWIR otoscopy can be used to examine the ossicular chain, cochlear promontory, round window niche, and chorda tympani. The ability to inspect the ossicular chain in greater detail could provide valuable diagnostic information in cases of conductive hearing loss such as in ossicular discontinuity or otosclerosis, a disorder characterized by abnormal bone growth. Imaging deeper within the middle ear can also allow evaluation of cholesteatoma extension within the middle

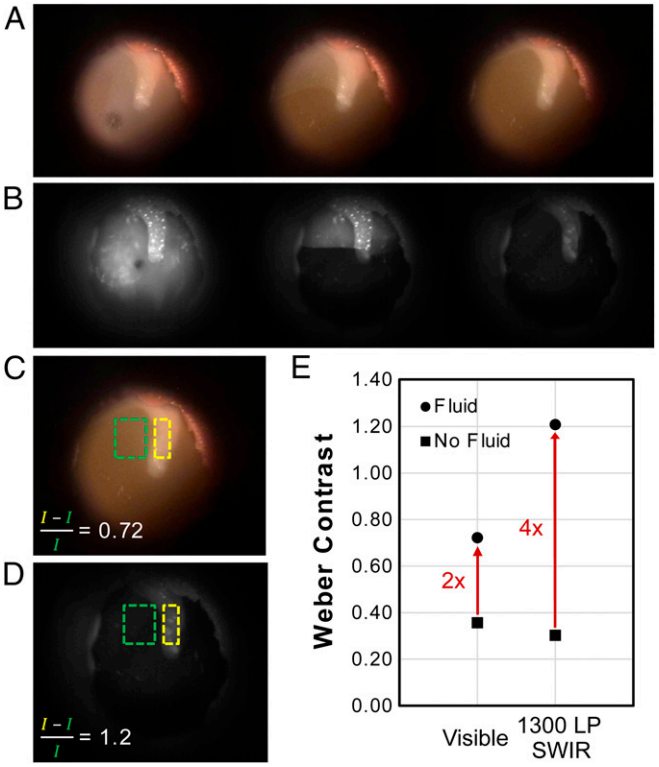

Fig. 5. Contrast between the presence and absence of fluid in a model middle ear with visible vs. SWIR otoscopy. As the model middle ear is filled with fluid phantom, a subtle intensity change behind the membrane can be observed using visible otoscopy (*A*). The SWIR otoscope provides a more striking contrast between presence and absence of fluid, particularly with a 1,300-nm long-pass filter that selectively passes the wavelengths of maximum fluid absorption (*B*). Monitoring the Weber contrast of the model structure shows that the contrast of this feature using SWIR otoscopy increases fourfold to 1.2 (*D*) compared with contrast in the absence of fluid of 0.30. This increase is a significant improvement over the twofold contrast increase from 0.36 to 0.72 observed using visible otoscopy (*C*). The Weber contrast for each case is plotted in *E*.

ear, especially in cases where the ossicular chain is suspected to be involved. The round window is used as an insertion site for cochlear implant electrodes and has also recently been used as an implantation site for hearing aid transducers (41–43). Clear visualization of the round window using a SWIR otoscope could provide an alternative to radiographic imaging for evaluation of such surgical implants. Thus, a SWIR otoscope has diagnostic potential in evaluating the cause of a variety of middle ear complications and in informing surgical procedures.

Furthermore, we predict that a SWIR otoscope can indicate middle ear effusions based on the strong light absorption of middle ear fluid beyond 1,300 nm. Otoscopy is the most widely used technology for assessing middle ear effusions; however, studies have shown that current visible light-based otoscopy is limited in accuracy, with correct interpretation by 46% of general practitioners, 51% of pediatricians, and 76% of otolaryngologists (28, 32, 44). Integrating SWIR light into otoscopy extends the available wavelengths to a regime in which endogenous contrast of middle ear fluid is much greater than at visible wavelengths. It should therefore provide a more objective determination of the presence or absence of middle ear effusion. Bringing objectivity to this diagnosis, which has long been plagued by diagnostic and therapeutic inconsistency, has the potential to reduce overprescription of antibiotics and unnecessary tympanostomy tube surgeries, which is the most common surgical procedure performed in US children (45). Potentially, an SWIR otoscope could also be used for differential detection of mucoid versus serous middle ear effusion, which is also of clinical interest. Measuring the attenuation of the middle ear at different wavelength regimes (e.g., 1,100 vs. 1,450 nm) simultaneously should enable distinction of thin vs. thick ear fluid with high accuracy, possibly giving a measure of the volumetric percentage of water in the fluid.

We underscore the importance of having a photonic method for direct visualization of the functional status of biological tissue. Tympanometry is an audiometric method shown to raise diagnostic success of otitis media to 83%; however, this method is not widely used in primary care settings, largely because nonspecialists lack training in this technique and are inhibited by the cost (28, 35, 46). Emerging technologies such as optical coherence tomography, spectral gradient acoustic reflectometry, and sonography have likewise shown potential for improving the diagnosis of otitis media, but thus far have not been widely adopted in general practice due to the difficulty of data interpretation or unfamiliarity of physicians with their use. (47–50) Using SWIR technology does not add time or complexity to a diagnosis and requires little additional training of medical practitioners who have already been trained in otoscopy. It is thus easily integrated into the clinic.

The general architecture of the SWIR otoscope, which provides immediate functional information, could be extended to the development of a variety of other medical devices to assist in a wide range of surgical procedures throughout the airway and gastrointestinal tract. Other disease conditions characterized by the buildup of fluid could be characterized by the enhanced contrast due to endogenous SWIR absorption. The SWIR otoscope is therefore only an initial example of how extending optical measurements into the SWIR can provide complimentary visual data and address existing limitations of conventional visible light-based medical devices.

Methods

Spectroscopy of Human Tympanic Membrane Tissue and Middle Ear Fluid. Human tympanic membrane tissue samples (~1-mm sections) were collected intraoperatively from pediatric patients (ages 0–18 y) during a typical tympanoplasty procedure. Human middle ear fluid samples (30- to 200-μL volumes) were collected intraoperatively from pediatric patients during myringotomy and placement of pressure-equalizing tubes for standard treatment of recurrent otitis media or persistent middle ear effusion. *SI Methods* provides information on sample collection, storage, and preparation details. Attenuation was measured using a Cary 5000 UV-VIS-NIR spectrophotometer (Varian/Agilent). All biospecimen sample collection and transfer procedures were approved by the Connecticut Children's Medical Center Institutional Review Board and were from volunteers who provided informed consent. Samples were used and characterized following the procedures approved by the Massachusetts Institute of Technology Committee on the Assessment of Biohazards and Embryonic Stem Cell Research Oversight and Biosafety Program.

SWIR Otoscope Design. The SWIR otoscope is composed of a fiber-coupled broadband halogen light source, a medical speculum that guides the device into the ear canal (Welch Allyn), speculums sized 2.5, 3.0, 4.0, or 5.0 mm), and a lens system to focus the diffusely reflected light onto an Indium Gallium Arsenide array detector. The lenses used in these experiments were from an Edmund Optics NIR achromatic lens pair with 75- and 100-mm effective focal length achromatic doublet lenses. The detector is a Xenics XS Trigger Indium Gallium Arsenide detector with a 320 × 256 array of 30-μm pixels and 14-bit analog-to-digital conversion resolution. A filter holder in front of the sensor allows easy adaptation with various short-pass, long-pass, and band-pass filters, enabling optimization of the device sensitivity for a variety of applications.

Human Middle Ear Imaging. The external auditory canal was used as the optical access for SWIR imaging of middle ear structures in both the left and right ears of healthy adults. The speculum was inserted into the canal within ~2 cm of the tympanic membrane and the middle ear was illuminated with the light source. Reflected light was collected by the optical system either broadband or filtered through a band-pass, long-pass, or short-pass filter. Visible images of the middle ear were taken of each subject in a similar manner (*SI Methods*). All participants provided informed consent and consent to publish images, and methods were carried out in accordance with the procedures approved by the Massachusetts Institute of Technology Institutional Review Board and Committee on the Use of Humans as Experimental Subjects, and Connecticut Children's Medical Center Institutional Review Board, and all procedures were in accordance with the Declaration of Helsinki guidelines.

Middle Ear Phantom. A middle ear phantom was 3D-printed using computer-assisted design software Solid Edge ST7 (Siemens). The shapes and angles were modeled to resemble the normal middle ear anatomical configuration based on previously described anatomical measurements (51). These models were used as the design files for the 3D printing process. A Makerbot Replicator Desktop 3D Printer (Makerbot Industries) was used with polylactic acid (PLA) as the printing filament. To model the semirigid and angled nature of the external auditory canal, a 3D-printed PLA cast was made, and high-performance platinum silicone (Dragon Skin FX-Pro; Smooth On) was used for the canal castings. The silicone was also cast into a thin, translucent sheet ~0.5 mm thick for the tympanic membrane and to line the inside of the 3D-printed PLA middle ear cavity, representing the mucosa of the cavity. A small hole in the back of the middle ear cavity was used to add fluid via a syringe into the phantom behind the silicone tympanic membrane while recording video using the SWIR or a visible otoscope inserted in the model canal.

ACKNOWLEDGMENTS. This work received support in part from the NIH through the Laser Biomedical Research Center, Grant 9-P41-EB015871-26A1 (to M.G.B.) and the Massachusetts Institute of Technology through the Institute for Soldier Nanotechnologies, Grant W911NF-13-D-0001 (to M.G.B.) and was conducted with government support under and awarded by the Department of Defense, Air Force Office of Scientific Research, National Defense Science and Engineering Graduate Fellowship 32 CFR 168a (to J.A.C.). O.T.B. was additionally supported by a European Molecular Biology Organization (EMBO) long-term fellowship.

1. Brown JQ, Vishwanath K, Palmer GM, Ramanujam N (2009) Advances in quantitative UV-visible spectroscopy for clinical and pre-clinical application in cancer. *Curr Opin Biotechnol* 20(1):119–131.
2. O'Sullivan TD, Cerussi AE, Cuccia DJ, Tromberg BJ (2012) Diffuse optical imaging using spatially and temporally modulated light. *J Biomed Opt* 17(7):071311-1–071311-14.
3. Wilson RH, et al. (2014) Quantitative short-wave infrared multispectral imaging of in vivo tissue optical properties. *J Biomed Opt* 19(8):086011-1–086011-4.
4. Bydlon TM, Nachabé R, Ramanujam N, Sterenborg HJCM, Hendriks BHW (2015) Chromophore based analyses of steady-state diffuse reflectance spectroscopy: Current status and perspectives for clinical adoption. *J Biophotonics* 8(1-2):9–24.

5. Jöbsis FF (1977) Noninvasive, infrared monitoring of cerebral and myocardial oxygen sufficiency and circulatory parameters. *Science* 198(4323):1264–1267.
6. Ferrari M, Giannini I, Sideri G, Zanette E (1985) Continuous non invasive monitoring of human brain by near infrared spectroscopy. *Adv Exp Med Biol* 191:873–882.
7. Murkin JM, Arango M (2009) Near-infrared spectroscopy as an index of brain and tissue oxygenation. *Br J Anaesth* 103(Suppl 1):i3–i13.
8. Valdez TA, et al. (2015) Multi-color reflectance imaging of middle ear pathology in vivo. *Anal Bioanal Chem* 407(12):3277–3283.
9. Lim YT, et al. (2003) Selection of quantum dot wavelengths for biomedical assays and imaging. *Mol Imaging* 2(1):50–64.
10. Nachabé R, Hendriks BHW, van der Voort M, Desjardins AE, Sterenborg HJCM (2010) Estimation of biological chromophores using diffuse optical spectroscopy: Benefit of extending the UV-VIS wavelength range to include 1000 to 1600 nm. *Biomed Opt Express* 1(5):1432–1442.
11. Hong G, et al. (2014) Through-skull fluorescence imaging of the brain in a new near-infrared window. *Nat Photonics* 8(9):723–730.
12. Wilson RH, Nadeau KP, Jaworski FB, Tromberg BJ, Durkin AJ (2015) Review of short-wave infrared spectroscopy and imaging methods for biological tissue characterization. *J Biomed Opt* 20(3):030901-1–030901-10.
13. Nachabé R, et al. (2011) Diagnosis of breast cancer using diffuse optical spectroscopy from 500 to 1600 nm: Comparison of classification methods. *J Biomed Opt* 16(8): 087010–087012.
14. Taroni P, Bargigia I, Farina A, Cubeddu R, Pifferi A (2011) First in vivo spectral characterization of breast up to 1300 nm. *Proc SPIE* 7896:78962L-1–78962L-4.
15. Akbari H, Uto K, Kosugi Y, Kojima K, Tanaka N (2011) Cancer detection using infrared hyperspectral imaging. *Cancer Sci* 102(4):852–857.
16. Akbari H, Kosugi Y, Kojima K, Tanaka N (2010) Detection and analysis of the intestinal ischemia using visible and invisible hyperspectral imaging. *IEEE Trans Biomed Eng* 57(8):2011–2017.
17. Randeberg LL, Skallerud B, Langlois NEI, Haugen OA, Svaasand LO (2010) The optics of bruising. *Optical-Thermal Response of Laser-Irradiated Tissue*, eds Welch AJ, van Gemert MJC (Springer, Dordrecht, The Netherlands), 2nd Ed, pp 825–858.
18. Randeberg LL, Hernandez-Palacios J (2012) Hyperspectral imaging of bruises in the SWIR spectral region. *Proc SPIE* 8207(N):82070N-1–82070N-10.
19. Altshuler GB, Anderson RR, Manstein D (2006) Method and apparatus for the selective targeting of lipid-rich tissues. Available at www.google.com/patents/US7060061. Accessed August 6, 2015.
20. Waxman S, Ishibashi F, Caplan JD (2007) Rationale and use of near-infrared spectroscopy for detection of lipid-rich and vulnerable plaques. *J Nucl Cardiol* 14(5):719–728.
21. Goldstein JA, et al. (2011) Detection of lipid-core plaques by intracoronary near-infrared spectroscopy identifies high risk of periprocedural myocardial infarction. *Circ Cardiovasc Interv* 4(5):429–437.
22. Bashkatov AN, Genina EA, Kochubey VI, Tuchin VV (2005) Optical properties of human skin, subcutaneous and mucous tissues in the wavelength range from 400 to 2000 nm. *J Phys Appl Phys* 38(15):2543–2555.
23. Bashkatov AN, Genina EA, Tuchin VV (2011) Optical properties of skin, subcutaneous, and muscle tissues: A review. *J Innov Opt Health Sci* 04(01):9–38.
24. Centers for Disease Control (2008) Table 2: Top 5 diagnoses at visits to office-based physicians and hospital outpatient departments by patient age and sex: United States 2008. Available at www.cdc.gov/nchs/data/ahcd/preliminary2008/table02.pdf. Accessed June 24, 2015.
25. Leibovitz E (2003) Acute otitis media in pediatric medicine: Current issues in epidemiology, diagnosis, and management. *Paediatr Drugs* 5(Suppl 1):1–12.
26. Soni A (2008) *Statistical Brief #228: Ear Infections (Otitis Media) in Children (0–17): Use and Expenditures, 2006* (Agency for Healthcare Research and Quality, Rockville, MD).
27. Teele DW, Klein JO, Rosner B (1989) Epidemiology of otitis media during the first seven years of life in children in greater Boston: A prospective, cohort study. *J Infect Dis* 160(1):83–94.
28. Abbott P, Rosenkranz S, Hu W, Gunasekera H, Reath J (2014) The effect and acceptability of tympanometry and pneumatic otoscopy in general practitioner diagnosis and management of childhood ear disease. *BMC Fam Pract* 15(1):181.
29. Rosser WW (1996) Approach to diagnosis by primary care clinicians and specialists: Is there a difference? *J Fam Pract* 42(2):139–144.
30. Pichichero ME (2003) Diagnostic accuracy of otitis media and tympanocentesis skills assessment among pediatricians. *Eur J Clin Microbiol Infect Dis* 22(9):519–524.
31. Pichichero ME, Poole MD (2001) Assessing diagnostic accuracy and tympanocentesis skills in the management of otitis media. *Arch Pediatr Adolesc Med* 155(10):1137–1142.
32. Pichichero ME, Poole MD (2005) Comparison of performance by otolaryngologists, pediatricians, and general practioners on an otoendoscopic diagnostic video examination. *Int J Pediatr Otorhinolaryngol* 69(3):361–366.
33. Powers JH (2007) Diagnosis and treatment of acute otitis media: Evaluating the evidence. *Infect Dis Clin North Am* 21(2):409–426, vi.
34. McGrath LJ, Becker-Dreps S, Pate V, Brookhart MA (2013) Trends in antibiotic treatment of acute otitis media and treatment failure in children, 2000-2011. *PLoS One* 8(12):e81210.
35. Garbutt J, Jeffe DB, Shackelford P (2003) Diagnosis and treatment of acute otitis media: An assessment. *Pediatrics* 112(1 Pt 1):143–149.
36. Pelton SI, Leibovitz E (2009) Recent advances in otitis media. *Pediatr Infect Dis J* 28(10, Suppl):S133–S137.
37. Rovers MM (2008) The burden of otitis media. *Vaccine* 26(Suppl 7):G2–G4.
38. Gupta A, Agarwal SR (1998) A study of prevalence of cholesteatoma in complications of suppurative otitis media. *Indian J Otolaryngol Head Neck Surg* 50(2):140–146.
39. Masanta WO, Hinz R, Zautner AE (2015) Infectious causes of cholesteatoma and treatment of infected ossicles prior to reimplantation by hydrostatic high-pressure inactivation. *BioMed Res Int* 2015:761259.
40. Rosenfeld RM (2002) Diagnostic certainty for acute otitis media. *Int J Pediatr Otorhinolaryngol* 64(2):89–95.
41. Skarzynski H, Lorens A, Piotrowska A, Anderson I (2007) Preservation of low frequency hearing in partial deafness cochlear implantation (PDCI) using the round window surgical approach. *Acta Otolaryngol* 127(1):41–48.
42. Erixon E, Köbler S, Rask-Andersen H (2012) Cochlear implantation and hearing preservation: Results in 21 consecutively operated patients using the round window approach. *Acta Otolaryngol* 132(9):923–931.
43. Colletti V, Soli SD, Carner M, Colletti L (2006) Treatment of mixed hearing losses via implantation of a vibratory transducer on the round window. *Int J Audiol* 45(10): 600–608.
44. Jones WS, Kaleida PH (2003) How helpful is pneumatic otoscopy in improving diagnostic accuracy? *Pediatrics* 112(3 Pt 1):510–513.
45. Kogan MD, Overpeck MD, Hoffman HJ, Casselbrant ML (2000) Factors associated with tympanostomy tube insertion among preschool-aged children in the United States. *Am J Public Health* 90(2):245–250.
46. Gates GA, Avery C, Cooper JC, Hearne EM, Holt GR (1986) Predictive value of tympanometry in middle ear effusion. *Ann Otol Rhinol Laryngol* 95(1 Pt 1):46–50.
47. Monroy GL, et al. (2015) Noninvasive depth-resolved optical measurements of the tympanic membrane and middle ear for differentiating otitis media. *Laryngoscope* 125(8):E276–E282.
48. Nguyen CT, et al. (2013) Investigation of bacterial biofilm in the human middle ear using optical coherence tomography and acoustic measurements. *Hear Res* 301: 193–200.
49. Puhakka T, Pulkkinen J, Silvennoinen H, Heikkinen T (2014) Comparison of spectral gradient acoustic reflectometry and tympanometry for detection of middle-ear effusion in children. *Pediatr Infect Dis J* 33(8):e183–e186.
50. Discolo CM, et al. (2004) Ultrasonic detection of middle ear effusion: A preliminary study. *Arch Otolaryngol Head Neck Surg* 130(12):1407–1410.
51. Hong P, et al. (2014) An anatomically sound surgical simulation model for myringotomy and tympanostomy tube insertion. *Int J Pediatr Otorhinolaryngol* 78(3): 522–529.
52. van Staveren HJ, Moes CJM, van Marie J, Prahl SA, van Gemert MJC (1991) Light scattering in Intralipid-10% in the wavelength range of 400-1100 nm. *Appl Opt* 30(31):4507–4514.
53. Pogue BW, Patterson MS (2006) Review of tissue simulating phantoms for optical spectroscopy, imaging and dosimetry. *J Biomed Opt* 11(4):41102–16.
54. Ninni PD, Martelli F, Zaccanti G (2011) Intralipid: Towards a diffusive reference standard for optical tissue phantoms. *Phys Med Biol* 56(2):N21–N28.